Article

High-resolution urban land-cover mapping and landscape analysis of the 42 major cities in China using ZY-3 satellite images

Xin Huang [a,b,*,1], Ying Wang [a,1], Jiayi Li [a], Xiaoyu Chang [a], Yinxia Cao [a], Junfeng Xie [c], Jianya Gong [a]

[a] School of Remote Sensing and Information Engineering, Wuhan University, Wuhan 430079, China
[b] State Key Laboratory of Information Engineering in Surveying, Mapping and Remote Sensing, Wuhan University, Wuhan 430079, China
[c] Land Satellite Remote Sensing Application Center, Ministry of Natural Resources of the People's Republic of China, Beijing 100048, China

ABSTRACT

Detailed and precise urban land-cover maps are crucial for urban-related studies. However, there are limited ways of mapping high-resolution urban land cover over large areas. In this paper, we propose an operational framework to map urban land cover on the basis of Ziyuan-3 satellite images. Based on this framework, we produced the first high-resolution (2 m) urban land-cover map (Hi-ULCM) covering the 42 major cities of China. The overall accuracy of the Hi-ULCM dataset is 88.55%, of which 14 cities have an overall accuracy of over 90%. Most of the producer's accuracies and user's accuracies of the land-cover classes exceed 85%. We further conducted a landscape pattern analysis in the 42 cities based on Hi-ULCM. In terms of the comparison between the 42 cities in China, we found that the difference in the land-cover composition of urban areas is related to the climatic characteristics and urbanization levels, e.g., cities with warm climates generally have higher proportions of green spaces. It is also interesting to find that cities with higher urbanization levels are more habitable, in general. From the landscape viewpoint, the geometric complexity of the landscape increases with the urbanization level. Compared with the existing medium-resolution land-cover/use datasets (at a 30-m resolution), Hi-ULCM represents a significant advance in accurately depicting the detailed land-cover footprint within the urban areas of China, and will be of great use for studies of urban ecosystems.

© 2020 Science China Press. Published by Elsevier B.V. and Science China Press. All rights reserved.

1. Introduction

Urbanization, which is characterized by a population shift from rural to urban and a transformation in the surface physical and geometric properties, has dramatically changed human habitats [1]. The evolution of the urban landscape has had a pronounced influence on the energy balance, carbon cycle, hydrological process, and climate of the urban systems [2,3]. Meanwhile, the accompanying problems include air and water pollution, the urban heat island (UHI) effect, environmental noise, and biodiversity reduction, which are threatening our health and future development [4–6]. Measuring and analyzing the urban landscape is thus essential for many applications in climatology, hydrology, environmental planning, and resource management, where detailed and precise urban land-cover maps are indispensable [7–9].

It is widely recognized that the satellite remote sensing technique can provide an effective tool for land-cover mapping at local,

regional, and global scales [10]. Several global land-use/cover datasets have been developed based on satellite images, with spatial resolutions of 300 m to about 1 km [11–14]. However, the drawbacks of these datasets are the coarse spatial resolutions, low accuracies, and poor agreement concerning time, space, and theme [15,16]. With the free availability of medium-resolution satellite images such as the Landsat and Sentinel series, more precise land-cover datasets with 10–30 m resolutions have become feasible. At the global level, the state-of-the-art products include the Finer Resolution Observation and Monitoring of Global Land Cover (FROM-GLC) maps [17], the Global Land Cover Dataset (GlobeLand30) [18], FROM-GLC-agg [19], and FROM-GLC10 [20]. At the regional level, the products include the European CORINE dataset [21], the United States National Land Cover Dataset (NLCD) [22], and the National Land Cover/Use Database of China (NLUD-C) [23]. Nevertheless, restricted by their spatial resolutions, none of these datasets can offer the necessary level of details within urban areas, such as individual buildings, sidewalks, and urban green spaces (e.g., roadside trees), which are crucial for the in-depth interpretation of the urban landscape. In this context, although the existing products are effective for the large-scale measurement

---

* Corresponding author.
  E-mail address: xhuang@whu.edu.cn (X. Huang).
[1] These authors contributed equally to this work.

and analysis of urban areas, they are still far from satisfactory for some urban planning and environmental analysis applications, due to the dearth of spatial details [8].

High-resolution satellite images can minimize the mixed-pixel phenomenon, and can thus provide abundant information in the spatial domain. Given their potential in delineating the structure and shape of individual objects (e.g., buildings, trees), high-resolution satellite images have been successfully applied in many urban-related studies, e.g., monitoring subtle urban dynamics [24], interpreting urban scenes [25], and investigating the effects of the landscape on the environment, such as the UHI effect [26]. Nevertheless, these studies were usually carried out in several small-size urban areas, for the purpose of classification algorithm analysis. To the best of our knowledge, to date, there has been very little practical research on techniques for high-resolution urban land-cover mapping over a large number of cities, and the related urban map products are also lacking.

The Ziyuan-3 (ZY-3) satellites are the first high-resolution civilian stereo mapping satellites in China, and the ZY-3 01 and ZY-3 02 satellites were successfully launched in 2012 and 2016, respectively. With a large swath width (50 km), the ZY-3 satellites can cover a large spatial extent with a spatial resolution of 2.1 m. The satellites are equipped with three high-resolution panchromatic cameras positioned 22° from each other to provide forward, nadir, and backward imaging modes, which enables them to provide abundant three-dimensional (3D) information to support accurate classification in complex urban scenes. Compared with other multi-angle high-resolution satellites (e.g., the WorldView series and the Cartosat series), the unique imaging mode of the ZY-3 satellites (along-track stereo mode with stable nadir-view cameras) enables them to provide nearly orthographic images, which can effectively minimize the angular effects, and therefore delineate urban surface cover more precisely. The angular effects can trigger distortion and occlusion of the land-cover maps, especially in urban scenes with complex high-rise structures, where the occlusion of buildings seriously hampers the accurate interpretation of the land-cover footprint [27]. With the available ZY-3 satellite imagery, we now have an unprecedented opportunity for mapping urban land cover.

In recent years, from the perspective of high-resolution image classification, auxiliary geospatial data has been increasingly utilized in land-use/cover classification, e.g., OpenStreetMap (OSM), open social data, and socioeconomic data [28,29]. However, the related studies have been carried out only at the local scale or in a small area, and we do not yet have an effective and feasible mapping scheme for large-scale use. In this context, we propose an operational mapping approach by integrating ZY-3 high-resolution satellite imagery and auxiliary geospatial data (A-map, Map World, and OSM). Under this framework, we developed a high-resolution (2 m) urban land-cover map (Hi-ULCM) covering the 42 major cities of China. China is currently undergoing urbanization at an unprecedented rate, and by the end of 2017, the urban population in China accounted for 58.52% [30], which is higher than the world average level (55%) [31]. During the past few years, significant land-cover changes have occurred in China [32], and a unified high-resolution land-cover map is urgently required. The Hi-ULCM dataset has the potential to fill this gap by providing detailed land-cover information of the urban areas. In this paper, based on this new land-cover dataset, the landscape patterns of the 42 major cities of China are analyzed and compared. Moreover, the potential of the Hi-ULCM dataset is fully discussed.

2. Materials and methods

In this study, we focused on the 42 major cities in China, including four municipalities, 26 provincial capitals, and 12 large cities (Fig. 1). These cities are spread over a wide range of climatic zones [33], and represent a variety of urban sizes, landscape characteristics, and urbanization intensities. The 42 cities were stratified into three levels according to the urban population in 2016 [34]: level I (greater than 5 million, 8 cities), level II (2 million to 5 million, 20 cities), and level III (<2 million, 14 cities) (Table S1 online). The 2015 NLUD-C dataset was adopted to extract the area of the municipal districts of the 42 cities [35], whose area and population are given in Table S1 (online), referring to the China City Statistical Yearbook for 2017. The NLUD-C dataset is a visually interpreted land-cover product derived from Landsat Thematic Mapper (TM), China-Brazil Earth Resources Satellite (CBERS), and HJ-1A images, with a spatial resolution of 30 m and an overall accuracy of more than 95% [23].

A total of 69 scenes of high-quality ZY-3 images acquired around 2015 were collected for the 42 cities. To make the vegetation conditions consistent, the acquisition dates of the ZY-3 images used in this study were limited to the growing season, i.e., from April to October (Table S1 online). As China's first high-resolution civilian stereo mapping satellite constellation, the deployment of two satellites (ZY-3 01 and ZY-3 02) significantly improves the data availability. Specifically, each satellite is equipped with panchromatic three-line array cameras (i.e., a nadir camera with a spatial resolution of 2.1 m, and two oblique cameras with spatial resolutions of 3.5 and 2.5 m for ZY-3 01 and ZY-3 02, respectively) and a multispectral camera with a 5.8-m resolution. Importantly, the availability of stable nadir images can minimize the angular effect and promote the accurate delineation of the urban surface cover. These merits make ZY-3 an excellent platform for providing high-resolution images for urban mapping. Apart from the satellite imagery, other geospatial data were also employed in the classification, including A-map, Map World, and OSM data. A-map and Map World are web map service providers of China, and they were used to supply the building footprint, road, and water area information in this research. OSM is a series of user-generated maps that are collaboratively edited by a large number of volunteers [36]. The quality of the geospatial data used in this study was evaluated from the perspective of positional accuracy, topological consistency, and completeness, by visual inspection [37].

A classification system consisting of seven representative land-cover categories was applied in this study: buildings, grass/shrubs (low vegetation), trees (tall vegetation), bare soil, water, roads, and other impervious surface areas (OISAs) (including squares, open areas, and pavements) [26]. The proposed framework is made up of four modules (Fig. 2): (1) pre-processing; (2) object extraction (for buildings, roads, and water) from ancillary data; (3) supervised classification (for grass/shrubs, trees, bare soil, and OISAs) from remote sensing imagery; and (4) land-cover map production and accuracy assessment.

In the pre-processing module, the digital surface model (DSM) was first generated from the ZY-3 stereo images (nadir and forward images were selected in this study) by the use of the semi-global matching (SGM) method [38]. Based upon the generated DSM, the panchromatic nadir ZY-3 imagery was then orthorectified. The multispectral images were then registered to the panchromatic nadir image, with a root-mean-square error (RMSE) of less than one pixel. Finally, the Gram-Schmidt pan-sharpening technique was performed to improve the spatial resolution of the multispectral images via fusing them with the panchromatic nadir image. Note that all the images were resampled to a uniform spatial resolution of 2.1 m. Using the pan-sharpened multispectral image as the benchmark, the multi-source geospatial data were spatially registered to it, and the RMSE was less than one pixel.

The geospatial data (A-map, Map World, and OSM) were then employed for identifying buildings, roads, and water. Buildings were obtained by synthesizing the A-map and Map World data.

Fig. 1. Spatial distribution of the 42 study sites within the five climatic zones in China. EW: equatorial climate and warm, fully humid temperate climate; W: warm temperate climate with dry winter; A: climate of arid steppe and desert; S: snow climate with dry winter; TS: tundra climate and snow climate with cool summer and cold winter.

Specifically, building footprints from A-map and Map World which were originally in vector form were converted to building objects. Footprints from A-map were utilized as the benchmark, that is, for the intersected or common objects (i.e., the building objects that appear on both A-map and Map World), the footprints from A-map were adopted. Map World served as the supplement for the omitted objects in A-map. Roads were a synthesis of the OSM road network and Map World data. Buffer zones were established, and the width of the buffer for each road was estimated by referring to both the road hierarchy (i.e., primary, secondary, tertiary, trunk, and motorway) of the OSM vectors and the corresponding ZY-3 imagery. Similarly, Map World was used to supplement OSM, especially for some pathways that were omitted in OSM. Water was extracted from Map World. In this way, the label images, consisting of the land-cover categories of buildings, roads, and water, could be generated.

Subsequently, the aforementioned three land-cover classes were applied as a mask layer to the ZY-3 imagery. The random forest (RF) classifier was performed to classify the remaining part of the imagery into the other four land-cover types (i.e., grass/shrubs, trees, bare soil, and OISAs) by taking the normalized DSM (nDSM), normalized difference vegetation index (NDVI), normalized difference water index (NDWI), and spectral features into account. RF is an ensemble classifier that uses classification and regression tree (CART) analysis to yield a prediction by majority voting [39]. Each tree is built by a randomly selected subset of variables and training samples. The attribute disturbance and sample disturbance increase the variation of the trees, contributing to a forest with

high variance and low deviation. Generally speaking, RF is regarded as a robust classifier [40]. For training the classifier, the number of trees ($Ntree$) was set to 100 and the number of features selected at each node ($Mtry$) was set to 3, as suggested by Belgiu and Drăguţ [40]. The nDSM, which delineates the height of objects above the Earth's surface by removing topographic effects, was derived from the DSM by morphological top-hat transformation [41]. The training and test samples were generated by *in-situ* investigation and visual inspection of the ZY-3 images and the corresponding higher-resolution Google Earth images. For each city, 80 polygons (each containing around 20 sample pixels) per class were selected to train the classifier, and around 200 pixels per class were randomly collected to assess the accuracy of Hi-ULCM. The test samples were independent of the training samples, and the minimum distance between test samples was 100 m, to ensure their independence and randomness. To guarantee the accuracy of the mapping, manual correction was conducted to further refine the classification results.

3. Results and validation

The Hi-ULCM product for two representative cities is presented in Fig. 3. We also provide the results for an additional four representative cities in Fig. S1 (online). These maps demonstrate that the footprint of the land cover, e.g., buildings, can be well depicted by the Hi-ULCM dataset. In particular, the product can delineate compact and small buildings, such as those found in urban villages and residential areas. Some buildings with low reflectance that are
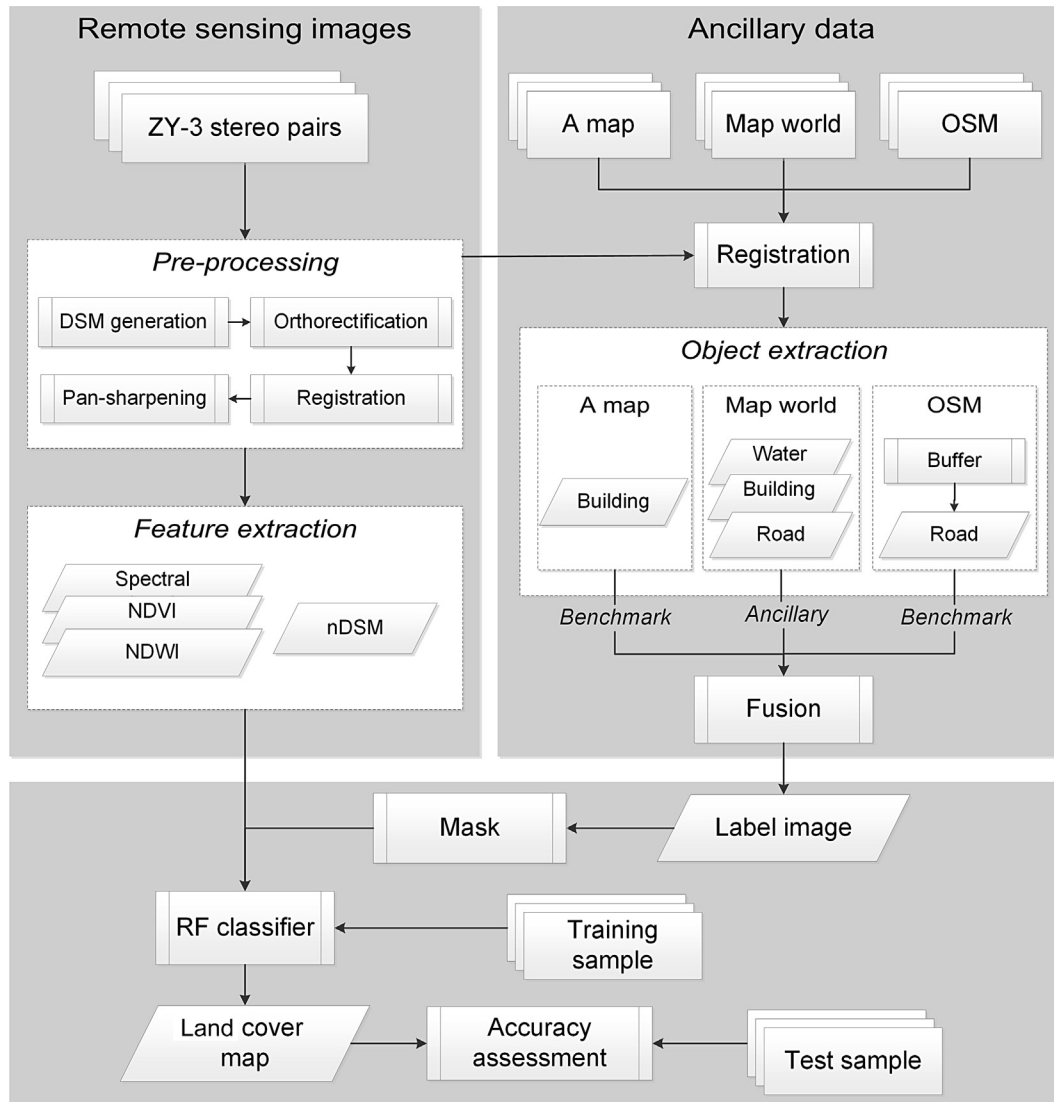
Fig. 2. The proposed framework for land-cover mapping using high-resolution ZY-3 images and geospatial data.

difficult to distinguish from the surrounding vegetation can also be easily identified. With respect to roads, Hi-ULCM can reveal their linear morphology, preventing them from being interrupted by the occlusion of roadside trees, which can be attributed to the combined use of OSM vector data and ZY-3 satellite data. Furthermore, the spectral, textural, and height features extracted from the ZY-3 imagery improves the separability of grass/shrubs and trees, leading to satisfactory classification results.

A total of 41,571 test samples were generated in the 42 cities. The confusion matrix calculated from the test samples is provided in Table 1, to indicate the overall accuracy (OA) of the map, along with the corresponding producer's accuracy (PA), user's accuracy (UA), and F1 score for each class, where PA and UA indicate the completeness and precision of the classification, respectively, and the F1 score represents a trade-off between PA and UA. The OA based on all the samples is 88.55%, with the PAs and UAs for all the land-cover classes (except for OISAs) being over 85%, suggesting very promising mapping results (Table 1), especially when considering the high spatial resolution and the large-scale dataset used in this research. The major difficulty arose from incorrectly identifying buildings, roads, and bare soil as OISAs. Consequently, the UA of OISAs is lower than that of the other land-cover classes.

These errors originated from a small number of faults in the vector data of buildings and roads, and also from the spatio-temporal mismatch between the vector products and the satellite images. These errors could be further mitigated through more intensive visual inspection. Compared with the artificial land-cover classes (i.e., buildings, roads, and OISAs), the natural land-cover classes present a higher accuracy. The results suggest that the Hi-ULCM product is able to meet the demand for the analysis of urban spatial patterns, since the accuracies for buildings (PA 86.93%, UA 86.25%) and roads (PA 92.14%, UA 89.63%), which are the basic components of urban scenes, can be regarded as satisfactory.

For individual cities, the OAs range from 85.38% (Haikou) to 94.34% (Hefei), of which very high accuracies (above 90%) are achieved in 14 cities (Table S2 online). With respect to the accuracy of each land-cover class (Fig. 4), expect for OISAs, the PA, UA, and F1 scores of the six land-cover classes all exceed 80%, with average values over 85%. When focusing on the F1 scores, the accuracies for roads, soil, trees, grass/shrubs, and water are all higher than 85% in the majority of the cities. For buildings, roads, trees, and water, there is not much difference between the PA and UA. However, the PAs for soil and grass/shrubs are significantly lower than the UAs, indicating that more omission errors exist than commission
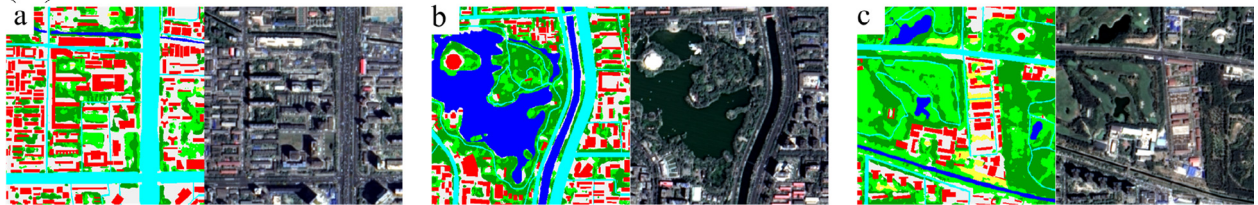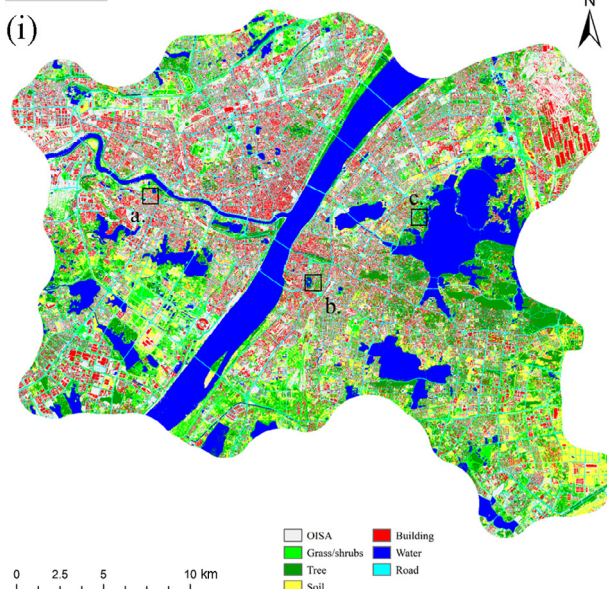
Beijing
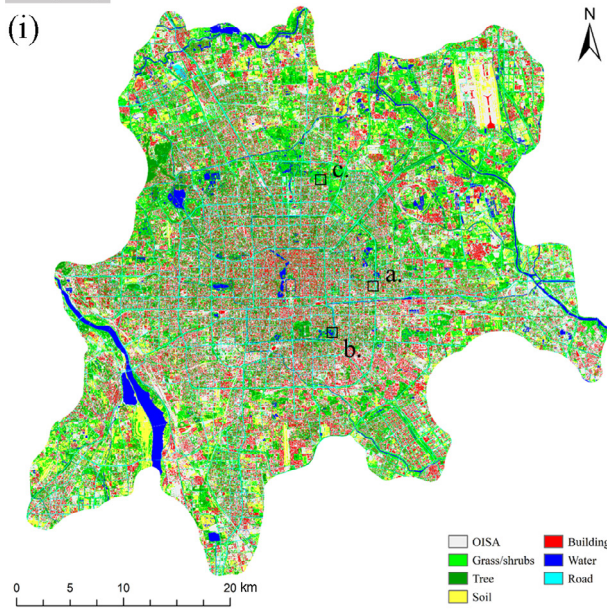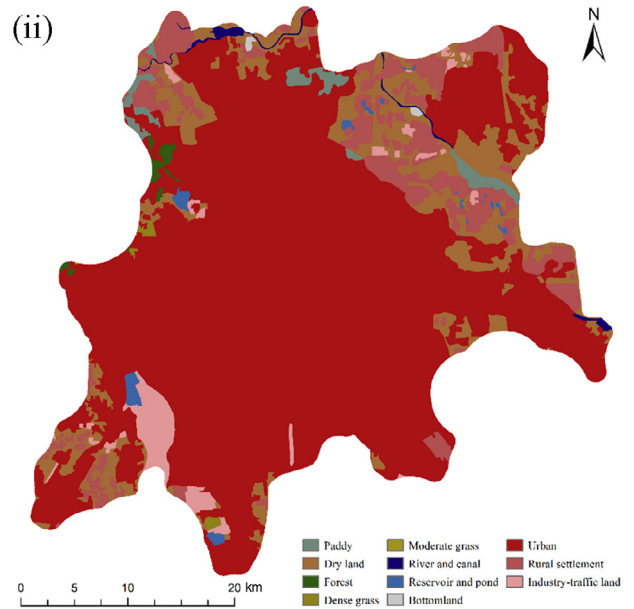
Wuhan

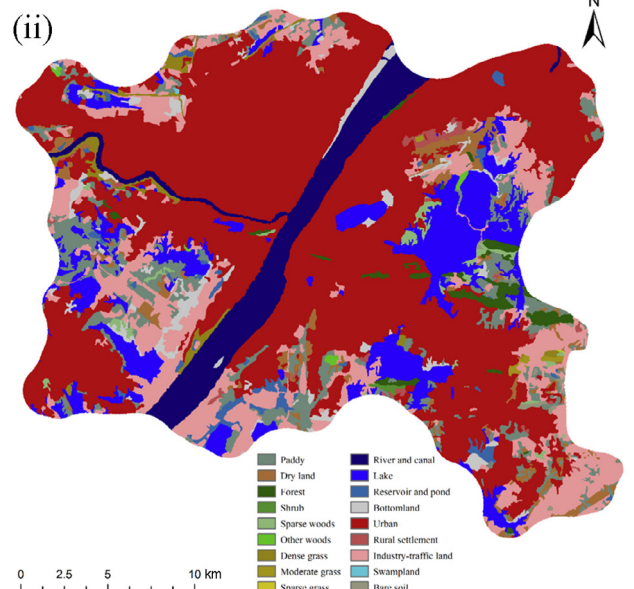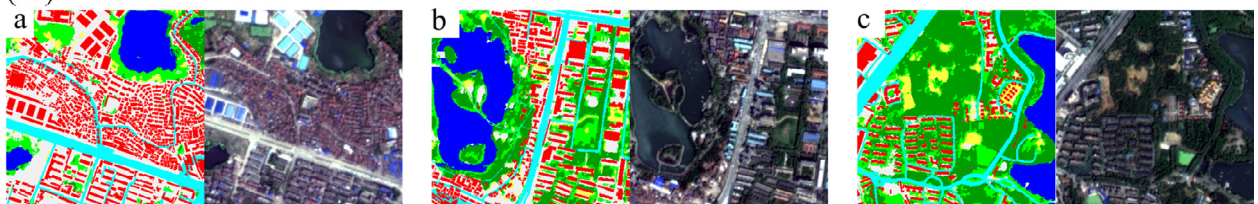**Fig. 3.** An illustration of Hi-ULCM (i), NLUD-C (ii), and close-up maps (iii) for some sample areas and the corresponding ZY-3 images in two representative cities: Beijing and Wuhan.

Table 1
Confusion matrix for the high-resolution land-cover dataset of the 42 cities.

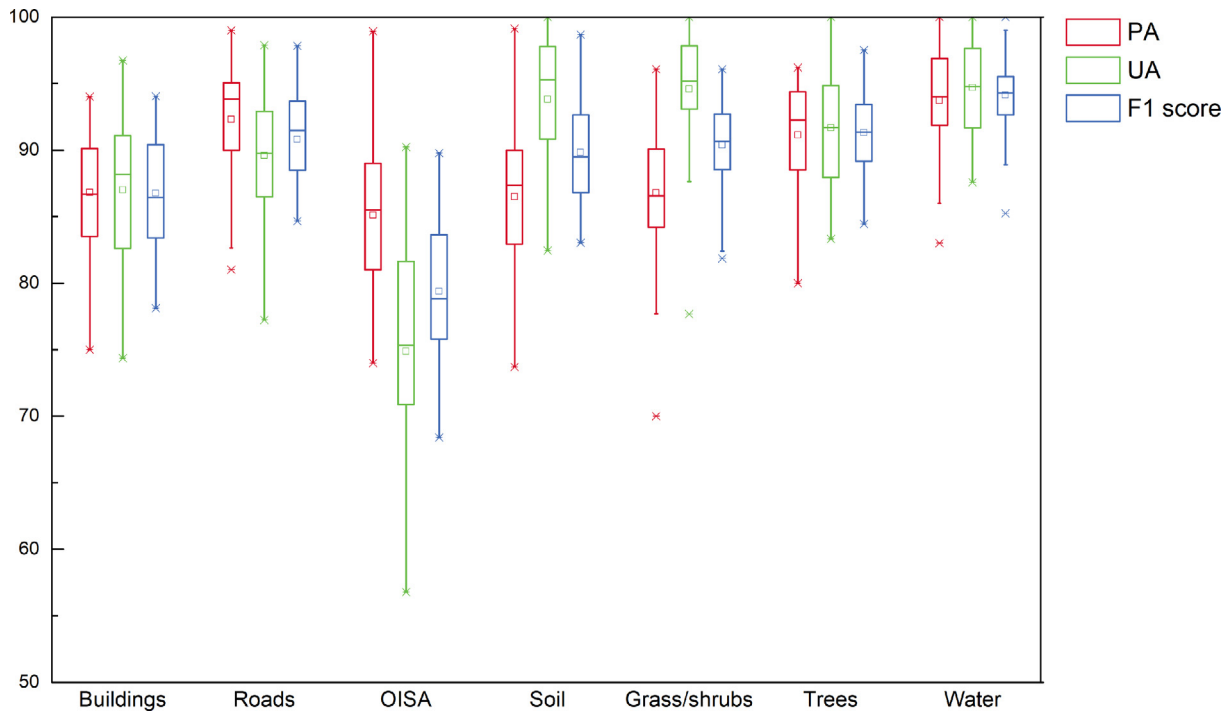|	Buildings	Roads	OISAs	Soil	Grass/shrubs	Trees	Water	UA (%)
Buildings	5728	18	401	291	129	64	10	86.25
Roads	34	5524	229	83	53	226	14	89.63
OISAs	668	383	5011	292	94	31	231	74.68
Soil	94	23	207	5105	39	12	11	92.97
Grass/shrubs	14	29	35	38	5229	189	24	94.08
Trees	39	10	8	9	437	5575	33	91.23
Water	12	8	25	92	79	40	4641	94.77
PA (%)	86.93	92.14	84.70	86.38	86.29	90.84	93.49	
OA (%)	88.55							

Fig. 4. Statistical results for the PA, UA and F1 scores in the 42 cities.

errors. These omission errors are partly from the soil pixels that were misclassified as OISAs, and the grass/shrubs misclassified as trees, due to their similar spectral reflectance. It can be seen from the length of the box (Fig. 4) that, except for OISAs, there is little variation in the accuracy among the 42 cities, implying fairly robust mapping results. Specifically, the PA, UA, and F1 scores of all the land-cover classes in each city are provided in Fig. S2 (online).

We made a comparison between the Hi-ULCM dataset and the 30-m resolution NLUD-C dataset (Fig. 3). The results of this comparison indicate that the most significant difference is that Hi-ULCM shows more spatial details in urban areas. Due to the lack of detailed land-cover information within the urban areas, as can be seen in Beijing (Fig. 3), NLUD-C shows little spatial information in built-up areas. Moreover, the urban green spaces, which have been proved to play a crucial role in environmental regulation (e.g., mitigating the UHI effect and urban noise [26,42]), also cannot be revealed by NLUD-C. In contrast, Hi-ULCM, which applies an urban-oriented land-cover classification system, performs well in characterizing detailed urban objects that are omitted in NLUD-C, such as buildings, roads, and urban green spaces. In addition, Hi-ULCM can better identify the small-size water bodies (e.g., Beijing in Fig. 3 and Xiamen in Fig. S1 online). To sum up, Hi-ULCM represents a great advance in accurately depicting the detailed

land cover of urban areas. The Hi-ULCM product is a high-resolution land-cover product dedicated to urban-related studies, which could be a valuable complement to the existing NLUD-C dataset.

4. Discussion

Based on the Hi-ULCM dataset, the land-cover composition of the 42 cities was analyzed with respect to the climatic zones (Fig. 5a) and city levels (Fig. 5b). The area percentage of OISAs is the largest among the 42 cities, with an average percentage of 27.49%, followed by buildings (16.23%), grass/shrubs (15.22%), trees (14.18%), roads (11.13%), soil (10.08%), and water (5.67%). The area percentages of artificial surfaces (i.e., buildings, roads, and OISAs) do not exhibit significant divergence in the different climatic zones. The proportion of green spaces is higher in cities with a warm climate (i.e., the EW and W climatic zones), accounting for 28.71% and 28.73%, respectively. In addition, most of the cities in the EW climatic zone are characterized by a higher proportion of water areas, whereas cities in the A climatic zone have higher proportions of bare soil. With respect to the city levels, the analysis of variance ($P < 0.05$) indicates that the composition of buildings and trees varies significantly in the three urban level groups. The proportion of buildings in level I is significantly lower than that in
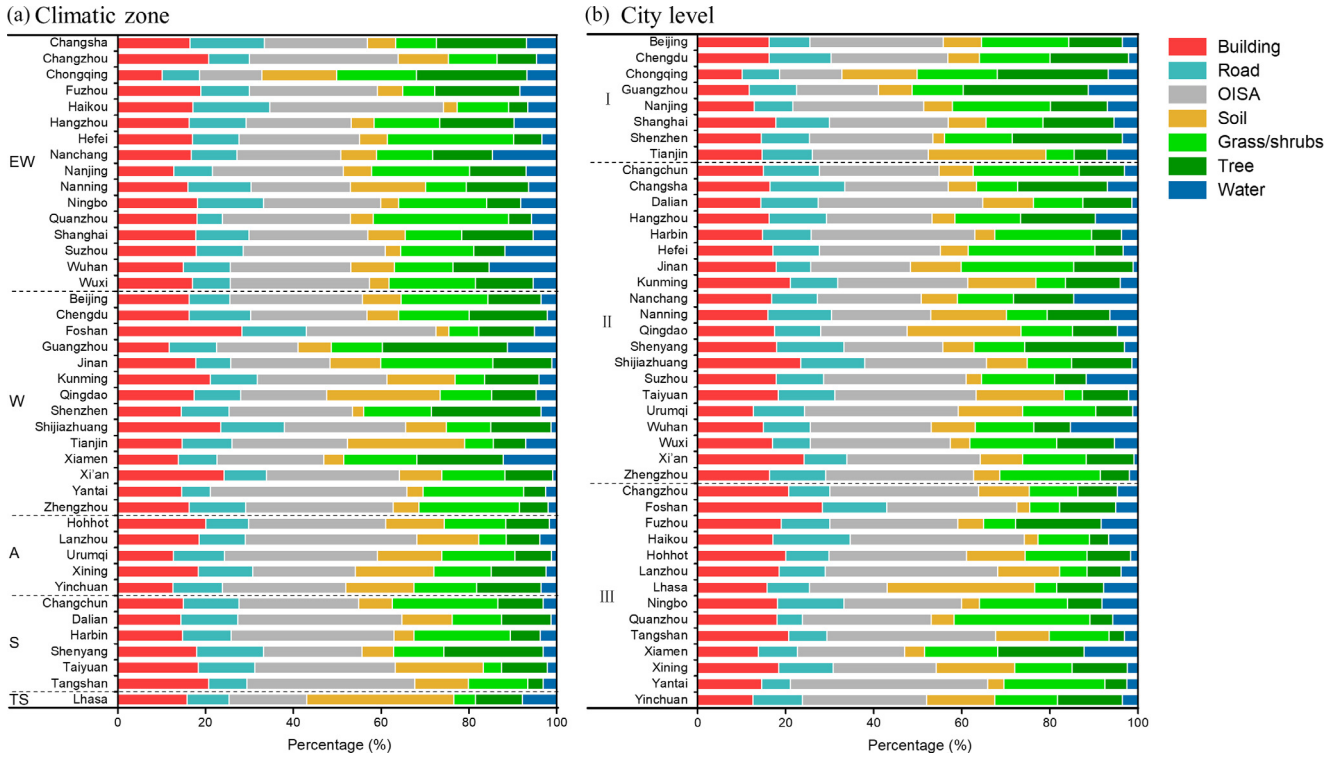
Fig. 5. Land-cover composition of the 42 cities in China, categorized by (a) climatic zones, and (b) city levels.

levels II and III. In contrast, the proportion of trees in the cities of level I is significantly higher than that in levels II and III, but the difference between levels II and III is not significant.

To further evaluate the amenities for residents in the 42 cities, we employed the ratio of open space (ROS) and the ratio of impervious space (RIS) to measure the porosity and intensity of artificial structures in the cities, respectively, where open space includes trees, grass/shrubs, and water, and impervious space includes buildings, roads, and OISAs [43]. Fig. 6a and b shows the relationships between the two landscape metrics and urban area (as urban area is a crucial indicator of urbanization). It can be seen that there is a significant positive relationship between urban area and ROS and a significant negative relationship between urban area and RIS. The possible reason for this is that, on the one hand, most of the cities with higher levels of urbanization are located in warm climatic zones with abundant precipitation, which is ideal for vegetation growth. On the other hand, with the development of urbanization, the government tends to pay more attention to public ecological space, and the importance of sustainable development is also highlighted.

In addition to land-cover composition, the Hi-NLUM dataset can also reveal the landscape configuration patterns of the urban areas. The complexity and dispersion of the urban landscape can be described by the landscape shape index (LSI) (Eq. (1) at the landscape level, and Eq. (2) at the class level), which has been proved effective in evaluating the geometric complexity of urban scenes [44,45]:

$$LSI = \frac{0.25E}{\sqrt{A}}, \tag{1}$$

$$LSI\_i = \frac{0.25\sum_{k=1}^{m}e_{ik}}{\sqrt{A}}, \tag{2}$$

where E and A are the total length of edge and total landscape area, respectively; and e_{ik} is the total length of edge in the landscape

between class i and k. The more complex and irregular the shape of the urban area, the higher the value of LSI. Fig. 6c–f demonstrates that LSI has a strong and positive linear correlation with urban area at both the landscape and class levels (for buildings, trees, and grass/shrubs). Studies based on medium- to low-resolution images have concluded that the shape complexity of built-up areas increases with urbanization [45,46]. In this study, we further found that the complexity and dispersion of the urban elements (i.e., buildings, trees, and grass/shrubs) also show increasing trends with the urbanization level. It is believed that a more complex and diffused urban shape is associated with a greater investment in infrastructure (e.g., pipeline networks and public transportation) and increased environmental risk (e.g., greenhouse gas emissions and degradation of natural resources) [46,47] and, consequently, the ecological and environmental effects of the fine-scale urban landscape patterns are worthy of further research.

Urban areas are hotspots that drive environmental change at local, regional, and global scales. Although the importance of urban ecology has been increasingly recognized, the relevant studies are still rather limited, partly due to the dearth of high-resolution urban land-cover maps covering large areas [1,48]. The Hi-ULCM dataset has the potential to address this data gap and to help us to further understand the ramifications of urbanization. Specifically, the Hi-ULCM product could be further applied to the following research aspects:

(1) The urban heat island (UHI) effect. The UHI effect is closely related to the surface biophysical characteristics in urban areas. However, most of the current knowledge of the contributors to the UHI effect is with regard to coarse land-cover types, such as vegetation and impervious surfaces, and urbanization dynamics, due to the lack of high-resolution images [35,49]. From the urban microclimate point of view, the interplay between the fine-scale urban landscape (e.g., building density and layout, and fragmentation of
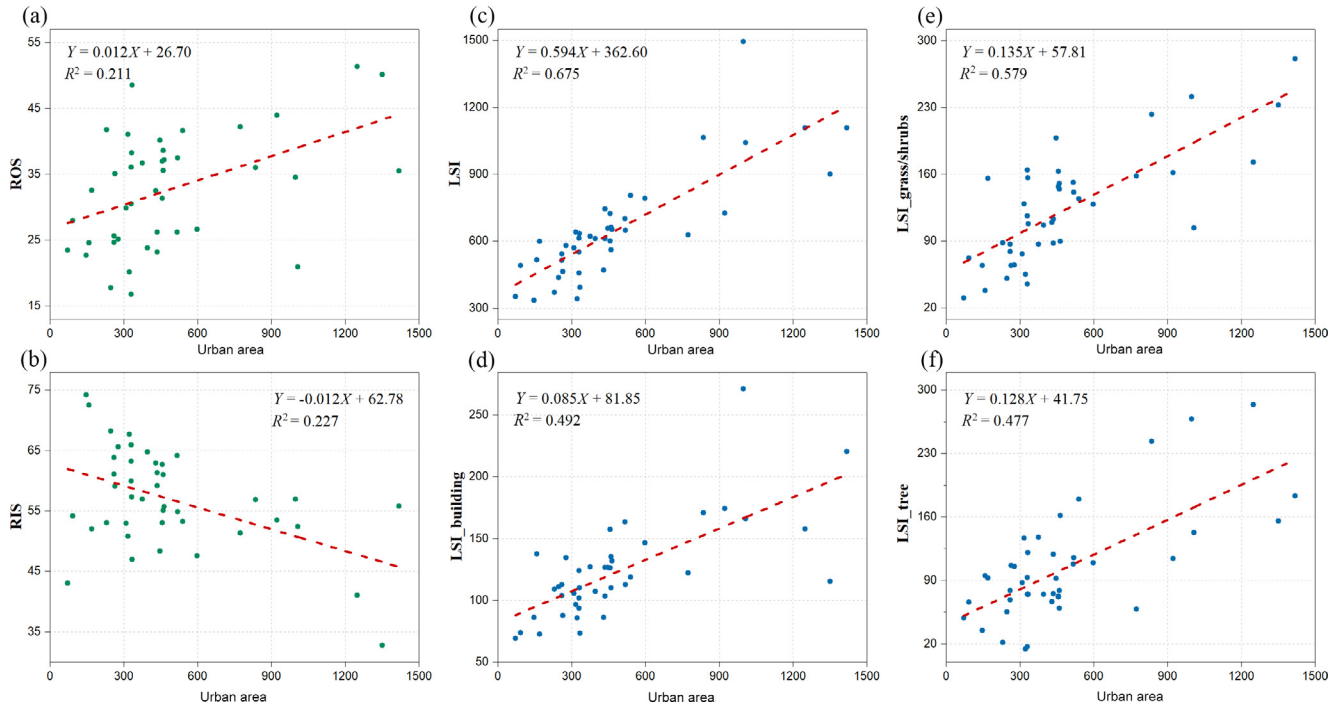
Fig. 6. The correlation between urban area and ROS (ratio of open space, (a)), RIS (ratio of impervious space, (b)), LSI (landscape shape index, (c)), LSI_building (d), LSI_grass/shrubs (e), and LSI_tree (f), respectively.

trees/grass) and the UHI effect is still unclear. The Hi-ULCM dataset will allow the discrimination of detailed individual urban elements and characteristics, so that it will be suitable for investigating the relationship between the fine-scale urban landscape and the UHI effect.

(2) Urban environmental pollution. Urban pollution, including both air pollutants (e.g., ozone, nitrogen oxide, and fine particulate matter ($PM_{2.5}$)) and environmental noise, has become of great concern because of its adverse impact on public health (e.g., coughs, asthma, and lung cancer) and mental stress [5,50]. Urban design can influence the formation, dispersion, and exposure to urban pollutants and noise via land cover, land use, and travel behavior [51]. The Hi-ULCM dataset could therefore contribute to the studies of the air and acoustic environments in terms of depicting detailed land cover and configurations (e.g., road networks), as well as being used to estimate anthropogenic emissions inventories [42,52].

(3) Deep learning (DL). DL has shown great potential in many applications (e.g., object detection, image classification, and scene understanding). However, it requires a substantial number of training samples to satisfy the network learning requirements, especially for high-resolution images [53]. From the algorithm development viewpoint, the Hi-ULCM dataset could be used to establish the correspondence between urban land cover and high-resolution images at the pixel level, based on the nadir-view images provided by the ZY-3 satellite, which could serve as a huge training pool for high-resolution land cover mapping. By using DL and transfer learning, we could develop a robust and transferable deep network for urban land-cover classification that could be adopted for other high-resolution images, to realize their automatic interpretation [54,55].

(4) Urban semantic scene classification. Urban semantic scene classification (i.e., labeling urban scenes with a set of semantic categories cognized and conceptualized by people) is crucial for urban environment and social analyses [56].

However, due to the heterogeneous patterns in high-resolution images, it is challenging to directly interpret the semantic labels from the images [57]. The Hi-ULCM dataset provides the basic land-cover classes in urban areas that can be applied to mine spatial semantic information and further identify the urban scenes, including land use, urban functional zones, and local climate zones, through spatial metrics, neighborhood graphs, and DL methods.

Apart from the applications discussed above, the Hi-ULCM dataset could also contribute to other social science research, such as sustainability assessment, habitat evaluation, risk and disaster assessment, energy consumption estimation, population estimation, and city health studies [58,59].

This study has opened a new avenue for producing high-resolution urban land-cover maps in a great number of cities. However, the current version of Hi-ULCM provides the land-cover product of the 42 largest cities in China. In our future work, we will supply the results for more cities to form a more holistic high-resolution urban land-cover product for China. In addition, we plan to update the product every five years, and to develop new methods to monitor the subtle urban land-cover changes [24]. On the other hand, in this study, we generated the nDSM derived from ZY-3 stereo images of the 42 cities to indicate the vertical information of the urban areas. However, there exists much uncertainty in the building height information estimated from the nDSM, due to the spatial precision of the ZY-3 satellites (i.e., spatial resolution and positioning accuracy) and the inherent difficulties of DSM generation (e.g., inaccurate image matching and incompleteness) [46]. In our future study, we will further improve the multi-view 3D reconstruction algorithm and estimate the building height from ZY-3 multi-view imagery accurately. As mentioned above, we will also try to apply Hi-ULCM to a variety of environmental and algorithm development applications. Other researchers are welcome to employ the Hi-ULCM dataset for the purpose of academic research, and we are willing to share the product when required.

5. Conclusion

In this paper, we have proposed an operational mapping framework for high-resolution urban land-cover mapping, and we have described the development of the first high-resolution (2 m) urban land-cover product—Hi-ULCM—covering the 42 major cities of China, courtesy of the high-resolution images acquired by the ZY-3 satellites. The proposed framework achieved a satisfactory performance, with an OA of 88.55%. Meanwhile, the PA and UA of each land-cover type exceeded 85%, for most of the categories. The landscape analysis indicated that the land-cover composition of the urban areas in China is related to the climatic characteristics and urbanization levels, e.g., cities with warm climates generally have higher proportions of green spaces. It is interesting to find that cities in level I are characterized by large proportions of open space areas (i.e., the sum of the tree, grass/shrubs, and water areas), suggesting that they could provide more amenities for residents. From the landscape viewpoint, it was revealed that the geometric complexity of the landscape (LSI) increases with the urbanization level, at both the landscape level and class level (for buildings, grass/shrubs, and trees).

Compared with the medium-resolution (30 m) NLUD-C land-cover/use dataset, the Hi-ULCM dataset represents a great advance in accurately depicting detailed land-cover footprints in urban areas. It can be regarded as a high-resolution version of the current NLUD-C dataset, and it has the potential to be used in a number of applications, e.g., studying the problems accompanying urbanization, such as the UHI effect and air and noise pollution; supporting algorithm development, such as transfer learning and DL; facilitating urban semantic scene classification; and many other social benefits. As a result, the Hi-ULCM dataset could help us to establish meaningful urban planning strategies to accommodate urban growth while improving the urban environment.

Conflict of interest

The authors declare that they have no conflict of interest.

Acknowledgments

Author contributions

Xin Huang and Jianya Gong conceived and supervised the work; Ying Wang, Jiayi Li, Xiaoyu Chang, and Yinxia Cao designed the method; Jiayi Li, Xiaoyu Chang and Yinxia Cao helped with the data processing; the remaining authors contributed collection of data and samples; all authors helped in writing the paper.

Appendix A. Supplementary materials

Supplementary materials to this article can be found online at https://doi.org/10.1016/j.scib.2020.03.003.

References

[1] Grimm NB, Faeth SH, Golubiewski NE, et al. Global change and the ecology of cities. Science 2008;319:756–60.

[2] Kalnay E, Cai M. Impact of urbanization and land-use change on climate. Nature 2003;423:528–31.

[3] Wang Y, Chen L, Kubota J. The relationship between urbanization, energy use and carbon emissions: evidence from a panel of association of Southeast Asian Nations (ASEAN) countries. J Clean Prod 2016;112:1368–74.

[4] Gong P, Liang S, Carlton EJ, et al. Urbanisation and health in China. Lancet 2012;379:843–52.

[5] Liu M, Liu X, Huang Y, et al. Epidemic transition of environmental health risk during China's urbanization. Sci Bull 2017;62:92–8.

[6] Yang J, Yan P, Li X. Urban biodiversity in China: who are winners? Who are losers? Sci Bull 2016;61:1631–3.

[7] Li X, Gong P. Urban growth models: progress and perspective. Sci Bull 2016;61:1637–50.

[8] Yang J, Wu T, Gong P. Implementation of China's new urbanization strategy requires new thinking. Sci Bull 2017;62:81–2.

[9] Liu X, Hu G, Chen Y, et al. High-resolution multi-temporal mapping of global urban land using Landsat images based on the google earth engine platform. Remote Sens Environ 2018;209:227–39.

[10] Dong J, Kuang W, Liu J. Continuous land cover change monitoring in the remote sensing big data era. Sci China Earth Sci 2017;60:2223–4.

[11] Bartholomé E, Belward AS. Glc 2000: a new approach to global land cover mapping from earth observation data. Int J Remote Sens 2005;26:1959–77.

[12] Friedl MA, Sulla-Menashe D, Tan B, et al. Modis collection 5 global land cover: algorithm refinements and characterization of new datasets. Remote Sens Environ 2010;114:168–82.

[13] Arino O, Gross D, Ranera F, et al. GlobCover: ESA service for global land cover from MERIS. Proceedings of the 2007 IEEE International Geoscience and Remote Sensing Symposium, 2007.

[14] Ran YH, Li X, Lu L, et al. Large-scale land cover mapping with the integration of multi-source information based on the Dempster-Shafer theory. Int J Geogr Inf Sci 2012;26:169–91.

[15] Herold M, Mayaux P, Woodcock CE, et al. Some challenges in global land cover mapping: an assessment of agreement and accuracy in existing 1 km datasets. Remote Sens Environ 2008;112:2538–56.

[16] Ran Y, Li X, Lu L. Evaluation of four remote sensing based land cover products over China. Int J Remote Sens 2010;31:391–401.

[17] Gong P, Wang J, Yu L, et al. Finer resolution observation and monitoring of global land cover: first mapping results with Landsat TM and ETM+ data. Int J Remote Sens 2013;34:2607–54.

[18] Chen J, Chen J, Liao A, et al. Global land cover mapping at 30 m resolution: a POK-based operational approach. ISPRS J Photogr Remote Sens 2015;103:7–27.

[19] Yu L, Wang J, Li X, et al. A multi-resolution global land cover dataset through multisource data aggregation. Sci China Earth Sci 2014;57:2317–29.

[20] Gong P, Liu H, Zhang M, et al. Stable classification with limited sample: transferring a 30-m resolution sample set collected in 2015 to mapping 10-m resolution global land cover in 2017. Sci Bull 2019;64:370–3.

[21] Büttner G. CORINE land cover and land cover change products. In: Manakos I, Braun M, editors. Land use and land cover mapping in Europe: practices & trends. London: Springer; 2014. p. 55–74.

[22] Homer C, Dewitz J, Yang L, et al. Completion of the 2011 national land cover database for the conterminous united states – representing a decade of land cover change information. Photogr Eng Remote Sens 2015;81:345–54.

[23] Zhang Z, Wang X, Zhao X, et al. A 2010 update of national land use/cover database of China at 1:100000 scale using medium spatial resolution satellite images. Remote Sens Environ 2014;149:142–54.

[24] Huang X, Wen D, Li J, et al. Multi-level monitoring of subtle urban changes for the megacities of China using high-resolution multi-view satellite imagery. Remote Sens Environ 2017;196:56–75.

[25] Huang X, Chen H, Gong J. Angular difference feature extraction for urban scene classification using ZY-3 multi-angle high-resolution satellite imagery. ISPRS J Photogr Remote Sens 2018;135:127–41.

[26] Huang X, Wang Y. Investigating the effects of 3d urban morphology on the surface urban heat island effect in urban functional zones by using high-resolution remote sensing data: a case study of Wuhan, central China. ISPRS J Photogr Remote Sens 2019;152:119–31.

[27] Matasci G, Longbotham N, Pacifici F, et al. Understanding angular effects in VHR imagery and their significance for urban land-cover model portability: a study of two multi-angle in-track image sequences. ISPRS J Photogr Remote Sens 2015;107:99–111.

[28] Zhao W, Bo Y, Chen J, et al. Exploring semantic elements for urban scene recognition: deep integration of high-resolution imagery and OpenStreetMap (OSM). ISPRS J Photogr Remote Sens 2019;151:237–50.

[29] Aubrecht C, Steinnocher K, Hollaus M, et al. Integrating earth observation and GIScience for high resolution spatial and functional modeling of urban land use. Comput Environ Urban Syst 2009;33:15–25.

[30] National Bureau of Statistics of China. China city statistical yearbook - 2018. Beijing: China Statistics Press; 2018.

[31] United Nations, Department of Economic and Social Affairs. World urbanization prospects: the 2018 revision. New York, 2018.

[32] Gong P, Li X, Zhang W. 40-Year (1978–2017) human settlement changes in China reflected by impervious surfaces from satellite remote sensing. Sci Bull 2019;64:756–63.
[33] Rubel F, Kottek M. Observed and projected climate shifts 1901–2100 depicted by world maps of the Koppen-Geiger climate classification. Meteorol Z 2010;19:135–41.
[34] Bai X, Shi P, Liu Y. Society: realizing China's urban dream. Nature 2014;509:158–60.
[35] Zhou D, Zhao S, Liu S, et al. Surface urban heat island in China's 32 major cities: spatial patterns and drivers. Remote Sens Environ 2014;152:51–61.
[36] Haklay M, Weber P. OpenStreetMap: user-generated street maps. IEEE Perv Comput 2008;7:12–8.
[37] Senaratne H, Mobasheri A, Ali AL, et al. A review of volunteered geographic information quality assessment methods. Int J Geogr Inf Sci 2017;31:139–67.
[38] Hirschmuller H. Stereo processing by semiglobal matching and mutual information. IEEE Trans Pattern Anal Mach Intell 2008;30:328–41.
[39] Breiman L. Random forests. Mach Learn 2001;45:5–32.
[40] Belgiu M, Drăguţ L. Random forest in remote sensing: a review of applications and future directions. ISPRS J Photogr Remote Sens 2016;114:24–31.
[41] Qin R, Fang W. A hierarchical building detection method for very high resolution remotely sensed images combined with DSM using graph cut optimization. Photogr Eng Remote Sens 2014;80:873–83.
[42] Han X, Huang X, Liang H, et al. Analysis of the relationships between environmental noise and urban morphology. Environ Pollut 2018;233:755–63.
[43] Huang J, Lu XX, Sellers JM. A global comparative analysis of urban form: applying spatial metrics and remote sensing. Landsc Urban Plann 2007;82:184–97.
[44] Schwarz N. Urban form revisited-selecting indicators for characterising European cities. Landsc Urban Plann 2010;96:29–47.
[45] Jia Y, Tang L, Xu M, et al. Landscape pattern indices for evaluating urban spatial morphology – a case study of Chinese cities. Ecol Indic 2019;99:27–37.
[46] Irwin EG, Bockstael NE. The evolution of urban sprawl: evidence of spatial heterogeneity and increasing land fragmentation. Proc Natl Acad Sci USA 2007;104:20672–7.
[47] Jia Y, Tang L. Environmental effects of the urban spatial form of Chinese cities. Acta Ecolog Sin 2019;39:2986–94.
[48] Zhou W, Fisher B, Pickett ST. Cities are hungry for actionable ecological knowledge. Front Ecol Environ 2019;17:135.
[49] Sun Y, Zhang X, Ren G, et al. Contribution of urbanization to warming in China. Nat Clim Chang 2016;6:706–9.
[50] Li X, Zhang Q, Zhang Y, et al. Attribution of $PM_{2.5}$ exposure in Beijing-Tianjin-Hebei region to emissions: implication to control strategies. Sci Bull 2017;62:957–64.
[51] Clark LP, Millet DB, Marshall JD. Air quality and urban form in U.S. Urban areas: evidence from regulatory monitors. Environ Sci Technol 2011;45:7028–35.
[52] Zheng B, Huo H, Zhang Q, et al. High-resolution mapping of vehicle emissions in China in 2008. Atmos Chem Phys 2014;14:9787–805.
[53] Li J, Huang X, Gong J. Deep neural network for remote-sensing image interpretation: status and perspectives. Natl Sci Rev 2019;6:1082–6.
[54] Liu H, Huang X, Wen D, et al. The use of landscape metrics and transfer learning to explore urban villages in China. Remote Sens 2017;9:365.
[55] Huang Z, Pan Z, Lei B. Transfer learning with deep convolutional neural network for SAR target classification with limited labeled data. Remote Sens 2017;9:907.
[56] Du S, Zhang F, Zhang X. Semantic classification of urban buildings combining VHR image and GIS data: an improved random forest approach. ISPRS J Photogramm Remote Sens 2015;105:107–19.
[57] Voltersen M, Berger C, Hese S, et al. Object-based land cover mapping and comprehensive feature calculation for an automated derivation of urban structure types at block level. Remote Sens Environ 2014;154:192–201.
[58] Yang B, Xu T, Shi L. Analysis on sustainable urban development levels and trends in China's cities. J Clean Prod 2017;141:868–80.
[59] Zhou YZ, Li X, Yang K, et al. Assessing the impacts of an ecological water diversion project on water consumption through high-resolution estimations of actual evapotranspiration in the downstream regions of the Heihe River basin. China Agric For Meteorol 2018;249:210–27.

Xin Huang is currently a Luojia Distinguished Professor of Wuhan University, China. He is the Founder of the Institute of Remote Sensing Information Processing, School of Remote Sensing and Information Engineering, Wuhan University. His research interests include remote sensing image processing methods and applications.

Ying Wang is currently pursuing the master's degree in the School of Remote Sensing and Information Engineering, Wuhan University. Her research interests include urban environment and urban land cover mapping.